π^0 photoproduction on the proton for photon energies from 0.675 to 2.875 GeV

M. Dugger,[1] B. G. Ritchie,[1] J. P. Ball,[1] P. Collins,[1] E. Pasyuk,[1] R. A. Arndt,[2] W. J. Briscoe,[2] I. I. Strakovsky,[2] R. L. Workman,[2] G. Adams,[31] M. Amarian,[29] P. Ambrozewicz,[12] E. Anciant,[7] M. Anghinolfi,[18] B. Asavapibhop,[24] G. Asryan,[40] G. Audit,[7] H. Avakian,[17,35] H. Bagdasaryan,[29] N. Baillie,[39] N. A. Baltzell,[34] S. Barrow,[13] M. Battaglieri,[18] K. Beard,[21] I. Bedlinskiy,[20] M. Bektasoglu,[28,29,*] M. Bellis,[5] N. Benmouna,[2] B. L. Berman,[2] N. Bianchi,[17] A. S. Biselli,[31,5] B. E. Bonner,[32] S. Bouchigny,[35,19] S. Boiarinov,[20,35] R. Bradford,[5] D. Branford,[11] W. K. Brooks,[35] S. Bültmann,[29] V. D. Burkert,[35] C. Butuceanu,[39] J. R. Calarco,[26] S. L. Careccia,[29] D. S. Carman,[35] B. Carnahan,[6] S. Chen,[13] P. L. Cole,[35,16] A. Coleman,[39,†] P. Coltharp,[13] D. Cords,[35,‡] P. Corvisiero,[18] D. Crabb,[38] H. Crannell,[6] J. P. Cummings,[31] E. De Sanctis,[17] R. De Vita,[18] P.V. Degtyarenko,[35] H. Denizli,[30] L. Dennis,[13] A. Deur,[35] K. V. Dharmawardane,[29] K. S. Dhuga,[2] R. Dickson,[5] C. Djalali,[34] G. E. Dodge,[29] J. Donnelly,[14] D. Doughty,[8,35] P. Dragovitsch,[13] S. Dytman,[30] O. P. Dzyubak,[34,§] H. Egiyan,[26,39,35] K. S. Egiyan,[40,‡] L. Elouadrhiri,[8,35] A. Empl,[31] P. Eugenio,[13] R. Fatemi,[38] G. Fedotov,[25] G. Feldman,[2] R. J. Feuerbach,[5] J. Ficenec,[37] T. A. Forest,[29] H. Funsten,[39] M. Garçon,[7] G. Gavalian,[26,40,29] G. P. Gilfoyle,[33] K. L. Giovanetti,[21] F. X. Girod,[7] J. T. Goetz,[3] R. W. Gothe,[34] K. A. Griffioen,[39] M. Guidal,[19] M. Guillo,[34] N. Guler,[29] L. Guo,[35] V. Gyurjyan,[35] C. Hadjidakis,[19] R. S. Hakobyan,[6] J. Hardie,[8,35] D. Heddle,[8,35] F. W. Hersman,[26] K. Hicks,[28] I. Hleiqawi,[28] M. Holtrop,[26] J. Hu,[31] M. Huertas,[34] C. E. Hyde-Wright,[29] Y. Ilieva,[2] D. G. Ireland,[14] B. S. Ishkhanov,[25] M. M. Ito,[35] D. Jenkins,[37] H. S. Jo,[19] K. Joo,[38,9] H. G. Juengst,[29,2] N. Kalantarians,[29] J. D. Kellie,[14] M. Khandaker,[27] K. Y. Kim,[30] K. Kim,[22] W. Kim,[22] A. Klein,[29] F. J. Klein,[35,6] A. V. Klimenko,[29] M. Klusman,[31] M. Kossov,[20] Z. Krahn,[5] L. H. Kramer,[12,35] V. Kubarovsky,[31] J. Kuhn,[5] S. E. Kuhn,[29] V. Kuznetsov,[22] J. Lachniet,[29] J. M. Laget,[7,35] J. Langheinrich,[34] D. Lawrence,[24] T. Lee,[26] A. C. S. Lima,[2] K. Livingston,[14] K. Lukashin,[6,35] J. J. Manak,[35] C. Marchand,[7] L. C. Maximon,[2] S. McAleer,[13] B. McKinnon,[14] J. W. C. McNabb,[5] B. A. Mecking,[35] M. D. Mestayer,[35] C. A. Meyer,[5] T. Mibe,[28] K. Mikhailov,[20] R. Minehart,[38] M. Mirazita,[17] R. Miskimen,[24] V. Mokeev,[25] K. Moriya,[5] S. A. Morrow,[7,19] V. Muccifora,[17] J. Mueller,[30] G. S. Mutchler,[32] P. Nadel-Turonski,[2] J. Napolitano,[31] R. Nasseripour,[34,12] S. Niccolai,[2,19] G. Niculescu,[21] I. Niculescu,[21] B. B. Niczyporuk,[35] M. Niroula,[29] R. A. Niyazov,[29,35] M. Nozar,[35] G. V. O'Rielly,[2] M. Osipenko,[18,25] A. I. Ostrovidov,[13] K. Park,[22] C. Paterson,[14] S. A. Philips,[2,¶] J. Pierce,[38] N. Pivnyuk,[20] D. Pocanic,[38] O. Pogorelko,[20] S. Pozdniakov,[20] B. M. Preedom,[34] J. W. Price,[3,4] Y. Prok,[23,35] D. Protopopescu,[14] L. M. Qin,[29] B. A. Raue,[12,35] G. Riccardi,[13] G. Ricco,[18] M. Ripani,[18] F. Ronchetti,[17] G. Rosner,[14] P. Rossi,[17] D. Rowntree,[23] P. D. Rubin,[33] F. Sabatié,[29,7] J. Slamanca,[16] C. Salgado,[27] J. P. Santoro,[6,35] V. Sapunenko,[18,35] R. A. Schumacher,[5] V. S. Serov,[20] A. Shafi,[2] Y. G. Sharabian,[40,35] J. Shaw,[24] S. Simionatto,[2] A. V. Skabelin,[23] E. S. Smith,[35] L. C. Smith,[38] D. I. Sober,[6] M. Spraker,[14] A. Stavinsky,[20] S. S. Stepanyan,[22] S. Stepanyan,[35,40] B. E. Stokes,[13] P. Stoler,[31] S. Strauch,[2,34] M. Taiuti,[18] S. Taylor,[32] D. J. Tedeschi,[34] U. Thoma,[15,35] R. Thompson,[30] A. Tkabladze,[2] S. Tkachenko,[29] L. Todor,[5] C. Tur,[34] M. Ungaro,[31,9] M. F. Vineyard,[36] A. V. Vlassov,[20] K. Wang,[38] L. B. Weinstein,[29] H. Weller,[10] D. P. Weygand,[35] M. Williams,[5] E. Wolin,[35] M. H. Wood,[24,34] A. Yegneswaran,[35] J. Yun,[29] L. Zana,[26] and J. Zhang[29]

(The CLAS Collaboration)

[1] *Arizona State University, Tempe, Arizona 85287-1504*
[2] *The George Washington University, Washington, DC 20052*
[3] *University of California at Los Angeles, Los Angeles, California 90095-1547*
[4] *California State University, Dominguez Hills, Carson, California 90747-0005*
[5] *Carnegie Mellon University, Pittsburgh, Pennsylvania 15213*
[6] *Catholic University of America, Washington, DC 20064*
[7] *CEA-Saclay, Service de Physique Nucléaire, F91191 Gif-sur-Yvette, France*
[8] *Christopher Newport University, Newport News, Virginia 23606*
[9] *University of Connecticut, Storrs, Connecticut 06269*
[10] *Duke University, Durham, North Carolina 27708-0305*
[11] *Edinburgh University, Edinburgh EH9 3JZ, United Kingdom*
[12] *Florida International University, Miami, Florida 33199*
[13] *Florida State University, Tallahassee, Florida 32306*
[14] *University of Glasgow, Glasgow G12 8QQ, United Kingdom*
[15] *Physikalisches Institut der Universitaet Giessen, 35392 Giessen, Germany*
[16] *Idaho State University, Pocatello, Idaho 83209*
[17] *INFN, Laboratori Nazionali di Frascati, 00044 Frascati, Italy*
[18] *INFN, Sezione di Genova, 16146 Genova, Italy*
[19] *Institut de Physique Nucleaire ORSAY, Orsay, France*

[20]Institute of Theoretical and Experimental Physics, Moscow, 117259, Russia
[21]James Madison University, Harrisonburg, Virginia 22807
[22]Kyungpook National University, 702-701 Daegu, South Korea
[23]Massachusetts Institute of Technology, Cambridge, Massachusetts 02139-4307
[24]University of Massachusetts, Amherst, Massachusetts 01003
[25]Moscow State University, General Nuclear Physics Institute, 119899 Moscow, Russia
[26]University of New Hampshire, Durham, New Hampshire 03824-3568
[27]Norfolk State University, Norfolk, Virginia 23504
[28]Ohio University, Athens, Ohio 45701
[29]Old Dominion University, Norfolk, Virginia 23529
[30]University of Pittsburgh, Pittsburgh, Pennsylvania 15260
[31]Rensselaer Polytechnic Institute, Troy, New York 12180-3590
[32]Rice University, Houston, Texas 77005-1892
[33]University of Richmond, Richmond, Virginia 23173
[34]University of South Carolina, Columbia, South Carolina 29208
[35]Thomas Jefferson National Accelerator Facility, Newport News, Virginia 23606
[36]Union College, Schenectady, New York 12308
[37]Virginia Polytechnic Institute and State University, Blacksburg, Virginia 24061-0435
[38]University of Virginia, Charlottesville, Virginia 22901
[39]College of William and Mary, Williamsburg, Virginia 23187-8795
[40]Yerevan Physics Institute, 375036 Yerevan, Armenia

Differential cross sections for the reaction $\gamma\ p \rightarrow p\ \pi^0$ have been measured with the CEBAF Large Acceptance Spectrometer (CLAS) and a tagged photon beam with energies from 0.675 to 2.875 GeV. The results reported here possess greater accuracy in the absolute normalization than previous measurements. They disagree with recent CB-ELSA measurements for the process at forward scattering angles. Agreement with the SAID and MAID fits is found below 1 GeV. The present set of cross sections has been incorporated into the SAID database, and exploratory fits have been extended to 3 GeV. Resonance couplings have been extracted and compared to previous determinations.

PACS numbers: 13.60.Le,14.20.Gk,13.30.Eg,13.75.Gx,11.80.Et

I. INTRODUCTION

The spectrum of baryon resonances has been extensively explored for clues to the internal structure of nucleons. Experimental and phenomenological programs are working in tandem to refine and expand the known resonance masses, widths, and electromagnetic couplings, which provide tight constraints for QCD-inspired models, and valuable benchmarks for lattice calculations. The most precisely determined resonance properties are associated with low-lying states and those higher-mass states with clear Breit-Wigner signatures in amplitudes where they contribute. Many other states have been observed, but with widely-varying mass and width estimates.

Much of the non-strange baryon spectrum has been deduced from fits to pion-nucleon scattering and photoproduction data. However there are difficulties encountered in extracting the states from experimental data. While many states have been predicted by QCD-inspired models, far fewer have been clearly identified. Some of these missing states may be weakly coupled to the pion-nucleon channel, and this possibility has motivated the study of other channels (involving ηN, $K\Lambda$, and $\pi\pi N$ final states, for example). Many of the states established in fits to elastic pion-nucleon scattering data have πN branching ratios [1] only of order 10-20% and therefore are not expected to be easily seen in πp elastic scattering. This is particularly true for resonances with masses above about 1.7 GeV.

Photodecay amplitudes can be extracted from fits to the available database of charged and neutral pion photoproduction data. A knowledge of the resonances contributing to pion-nucleon elastic scattering is crucial in this task. Precise measurements of the cross section and polarization asymmetries are equally important. However, until very recently, such measurements were lacking in the region above 1 GeV in photon energy. Recent Jefferson Lab measurements have shown that surprises are possible in the behavior of both polarized [2] and unpolarized [3] cross sections. Present fits covering photon energies to 2 GeV and beyond are necessarily model-dependent and underconstrained.

In this paper, we report measurements of the unpolarized differential cross sections of neutral pion photoproduction on the proton for incident photon energies from 0.675 to 2.875 GeV. We have included the present set

*Present address: Sakarya University, Sakarya, Turkey
†Present address: Systems Planning and Analysis, Alexandria, Virginia 22311
‡Deceased.
§Present address: Department of Radiology, Mayo Clinic College of Medicine, Rochester, MN 55905
¶Present address: Canberra Industries, Meriden, Connecticut 06457

of CLAS cross sections in a multipole fit to the available data covering the resonance region. At the highest energies, recent CB-ELSA [4] measurements are available, and we have compared both data and fits to show where deviations occur. Resonance couplings have been extracted for those states that give a significant contribution to the photoproduction process. In some cases, these couplings differ significantly from previous determinations.

The paper is laid out in the following manner: We give a brief overview of the experiment in Section II. A more detailed examination of methods used in the data reduction follows in Section III. The uncertainty estimates for the cross sections obtained are given in Section IV. The experimental results are described in Section V. Various fits to the data are described in SectionVI, and the underlying multipole amplitudes and resonance contributions are displayed and compared to previous determinations in Section VII. Finally, in Section VIII, we provide a brief summary of the results of this study and consider what extensions of this work would be particularly helpful in the future.

II. EXPERIMENT

The differential cross sections for the reaction $\gamma\ p \rightarrow p\ \pi^0$ were measured with the CEBAF Large Acceptance Spectrometer (CLAS) [5] and the bremsstrahlung photon tagging facility ("photon tagger") [6] in Hall B of the Thomas Jefferson National Accelerator Facility (JLab) as part of a set of experiments running at the same time with the same experimental configuration (cryogenic target, tagger, and CLAS) called the "$g1c$" run period. The cross sections can be found in electronic form in Ref. [7] and were part of a program of meson photoproduction measurements undertaken using the CLAS and photon tagger [8, 9, 10, 11, 12, 13, 14, 15]. The database entries include the differential cross sections, as well as uncertainties (excluding the overall absolute normalization uncertainty), for each incident photon energy and $\cos\theta^{\pi}_{\rm c.m.}$ shown in this document.

The full data described here consisted of two running periods with different incident electron beam energies of 2.445 and 3.115 GeV. Tagged photons were incident on an 18-cm-long liquid hydrogen target placed at the center of CLAS. This target was enclosed by a scintillator array (start counter) that detected the passage of charged particles into CLAS from the target [16]. The event trigger required the coincidence of a post-bremsstrahlung electron passing through the focal plane of the photon tagger and at least one charged particle detected in CLAS and the start counter. Tracking of the charged particles through the magnetic field within CLAS by drift chambers provided determination of their charge, momentum, and scattering angle. This information, together with the particle velocity measured by the time-of-flight system [17] and start counter, provided particle identification for each particle detected in CLAS and its corresponding momentum four-vector. The methods used for extracting the differential cross sections for π^0 photoproduction are presented in the next several sections. The technique is outlined initially, and then each step is described in further detail, with data and tests that support the validity of the approach.

III. DATA REDUCTION

Yields for the π^0 mesons resulting from photoproduction on the protons within the cryogenic hydrogen target were determined using the missing mass technique, assuming the two-body reaction $\gamma\ p \rightarrow p\ X$, where X is the particle hypothesized to be missing. Briefly, the following steps are involved in this analysis:

1. Identify the recoil proton in CLAS, determining the scattering angle and momentum for the proton.

2. Calculate the missing mass for the recoil proton based on the assumption that the reaction observed is $\gamma\ p \rightarrow p\ X$.

3. Distribute the events of the resulting missing mass spectra into bins defined by incident photon energy E_γ and π^0 center-of-mass scattering angle $\cos\theta^{\pi}_{\rm c.m.}$, based on the assumption that the reaction observed is $\gamma\ p \rightarrow p\ \pi^0$.

4. Identify the π^0 meson missing mass peak.

5. Determine the yield for the π^0 meson by subtracting any background from beneath the meson peak.

6. Correct the meson yield for spectrometer acceptance and detection efficiency based on Monte Carlo estimates of those quantities. This Monte Carlo technique was compared to empirical measurements of the CLAS acceptance and detection efficiency for a single proton, using measurements of the reaction $\gamma\ p \rightarrow p\ \pi^-\ \pi^+$ made concurrently with the data discussed here, to validate the Monte Carlo simulation used.

7. Normalize the yield using a measured absolute photon flux normalization procedure.

In the following sections, each of these steps is described. Also presented are sample results, and, in some cases, tests that establish the validity of the procedures used.

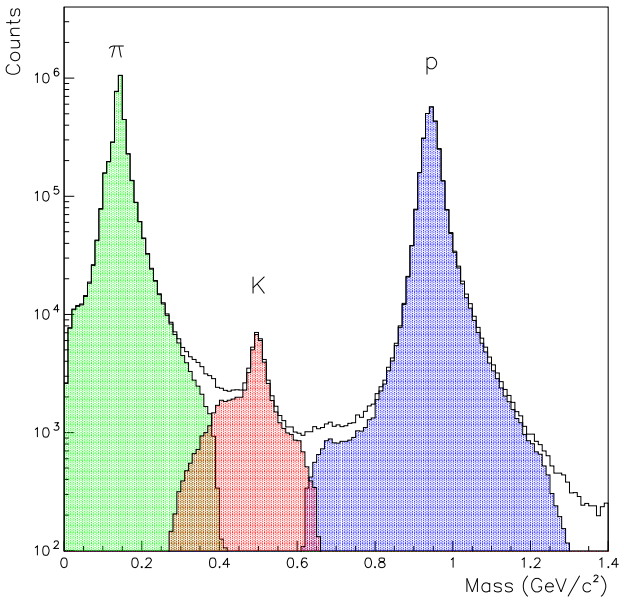

FIG. 1: Mass distribution of the detected charged hadrons (note logarithmic scale).

A. Recoil proton and pion identification; kinematic variables

The tracking information provided by the drift chambers within CLAS gave momentum and scattering angle information on charged particles scattered within the detector volume. Time-of-flight and start counter information, coupled with the track information provided by the drift chambers, yielded velocity and momentum determination.

Particle identification in this analysis was performed using the GPID algorithm [18]. The method uses the momentum of the detected particle, and sequentially calculates trial values of β for the particle for possible particle identities. Each one of the possible identities is tested by comparing the trial value of β for a given particle type to the empirically measured value of β (as determined by CLAS tracking and time-of-flight information). The particle is assigned the identity that provides the closest trial value of β to the empirically measured value of β. Figure 1 shows the mass distribution of the identified positively charged particles. The GPID algorithm also attempts to find a matching photon in the tagging system for every charged particle detected in CLAS. A matched photon means that there was one and only one tagged photon in the trigger window, which, in this analysis, is defined as being within the trigger coincidence window. Particles that are determined not to have a matching photon are considered to be a measure of the accidentals (to be described in more detail in the next subsection).

Geometrical fiducial cuts in each of the six sectors of CLAS were imposed on all protons. The region selected for accepting protons in each sector corresponded to a region of relatively uniform detection efficiency versus azimuthal angle.

B. Missing mass reconstruction

The momentum determined by CLAS was corrected for energy loss within the cryogenic target cell to reconstruct the momentum of the detected proton at the reaction vertex within the cryogenic target. In addition to the energy loss correction, a further momentum and photon energy correction developed by Williams *et al.* [19] for $g1c$ data was applied. (This second momentum correction was required to correct for problems with the magnetic field map associated with the CLAS detector.) The measured scattering angle and momentum can be used to construct a missing mass based on the assumption that the reaction observed is $\gamma\ p \rightarrow p\ X$, where X is the undetected particle in the two-body final state. Based on this assumption, the missing mass spectrum of the full spectrometer acceptance for all photon energies is shown in Fig. 2. The η, ρ^0/ω, and η' peaks are clearly seen atop a background dominated by multi-pion events. The π^0 peak is clearly discernible.

Taking each proton event that did not have a matching incident photon as noted above, and integrating over all of the out-of-time (not within the trigger coincidence window) incident photons for that event, determined the distribution of accidental coincidences between the CLAS and the photon tagger, under the assumption that coupling the out-of-time tagger events for each non-matched proton created a fair representation of the accidental coincidences between the CLAS and tagger.

A failure to match a particle to an incident photon mainly occurs when reconstructed timing information for the track or tagging system is missing.

C. Distribution of events into kinematic bins

The events, from the 2.445 and 3.115 GeV data sets, constituting the full missing mass spectrum described in the previous section were distributed into bins in photon energy E_γ and $\cos\theta^\pi_{\rm c.m.}$. The widths of these "kinematic bins" ($\Delta E_\gamma = 50$ MeV in photon energy and $\Delta\cos\theta^\pi_{\rm c.m.} = 0.1$) were chosen such that, in general, there were at least 1000 π^0 events in each kinematic bin.

D. Determination of pion yield within each kinematic bin

The π^0 yield within each kinematic bin was determined by subtracting the background under the peak in the missing mass spectrum. We proceeded with the assump-

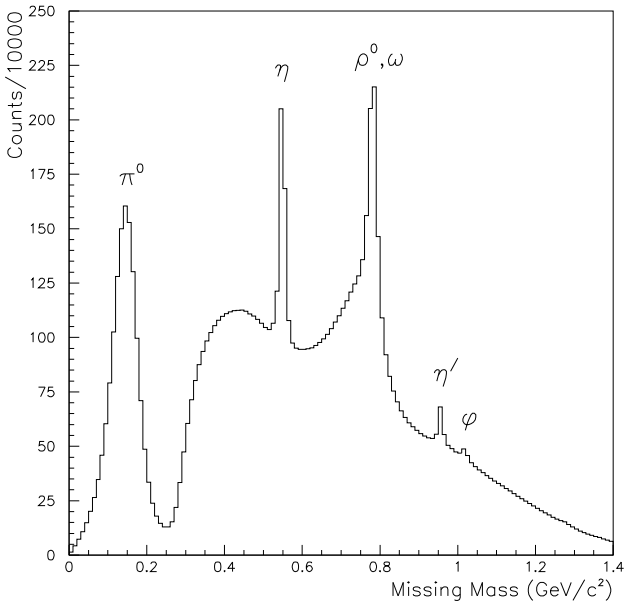

FIG. 2: Missing mass spectra obtained using CLAS, assuming the reaction $\gamma\ p \rightarrow p\ X$.

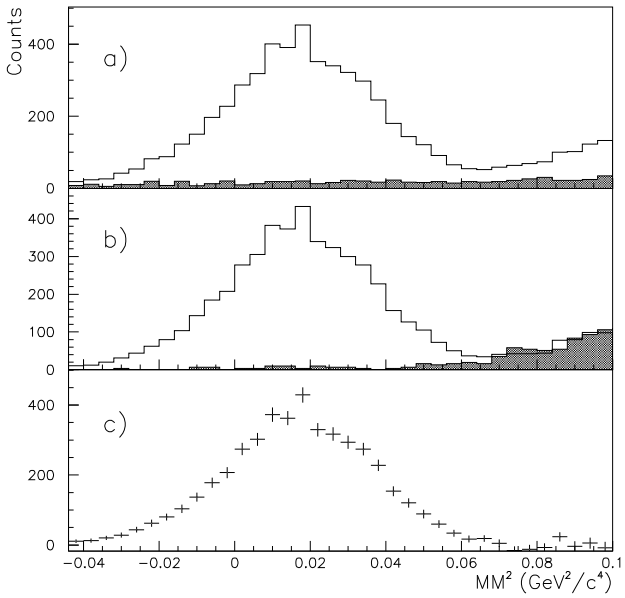

FIG. 3: π^0 meson yield extraction for the kinematic bin with $E_\gamma = 1.425$ GeV and $\cos\theta^{\pi}_{\rm c.m.} = 0.45$. The top panel a) is the missing mass yield for this bin, with the accidental contribution displayed as a shaded region. The middle panel b) shows the missing mass distribution with the accidentals subtracted, and the shaded region represents the 2π contribution. The bottom panel c) shows the extracted π^0 yield after both contributions have been subtracted from the missing mass distribution.

tion that the background in the missing mass spectra arose from two particular sources:

1. Accidental coincidences between CLAS and the photon tagger.

2. Two pion photoproduction via the reaction $\gamma\ p \rightarrow p\ X$, where $X = \pi^+\pi^-$.

The accidental contributions to each kinematic bin were determined as described in Section III.B. Since events with $p\pi^+\pi^-$ final states were copiously produced in this experiment (as may be seen in Fig. 2), the shape of the low energy portion of the 2π background contribution could be reliably determined. This shape was used to generate the background beneath the π^0 peak, which was then subtracted from the π^0 yield for each kinematic bin. An example of the individual contributions to the background beneath the pion peak can be seen in Fig. 3.

E. Acceptance and efficiency

The CLAS detector acceptance and detection efficiency for recoil protons were measured and then compared to a Monte Carlo simulation. The reaction used to determine the empirical acceptance and efficiency of protons in CLAS was $\gamma\ p \rightarrow p\ \pi^-\ \pi^+$. This reaction was used due to the high number of events for that final state and, since all the final products leave charged tracks in the CLAS, these events are easily observed. Both pions were required to be detected in the event and both matched to the same photon.

The data used for the empirical acceptance and efficiency calculations included only events where two and only two charged pions were detected in the CLAS. For each event, a missing mass reconstruction from the kinematical information from the two pions was performed to determine if a proton should have been seen in the CLAS. As shown in Fig. 4, the proton generally was very cleanly defined, so that the determination that a proton should have been seen could be made without ambiguity. The background beneath this peak was approximated by a third order polynomial and subtracted. The same fiducial cuts applied to the protons noted above were applied to both reconstructed and CLAS-identified protons.

The proton acceptance and efficiency α empirically determined in this fashion is the ratio of the number of protons "seen" N_s (i.e., identified in CLAS through the normal particle identification procedure, GPID, in the empirical data set) and the total number of events N_p where a proton should have been seen, based on reconstructed four-vectors from the pions, detected in the same subset of events.

A comparison of Monte Carlo events to actual data for the $\gamma\ p \rightarrow p\ \pi^-\ \pi^+$ reaction (rebinned for the $\gamma\ p \rightarrow p\ \pi^0$ reaction) was performed. Simulated events were obtained by generating 10^7 $\gamma\ p \rightarrow p\ \pi^-\ \pi^+$ events that were

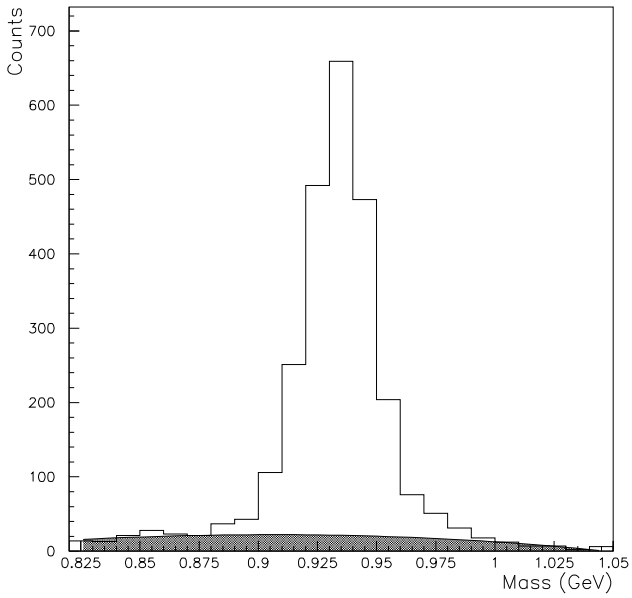

FIG. 4: Missing mass (mass of X) for the reaction $\gamma\ p \rightarrow \pi^-\ \pi^+ X$ near the mass of the proton (shaded region represents the background).

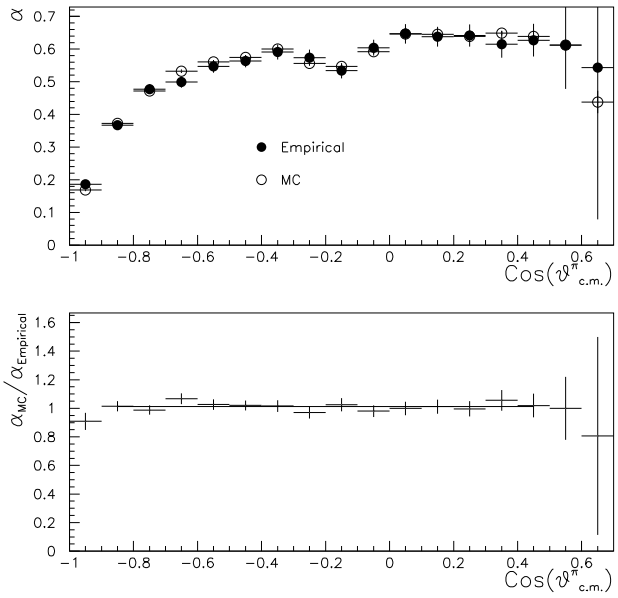

FIG. 5: Empirical and Monte Carlo acceptance and efficiencies α for π^0 photoproduction for $E_\gamma = 725$ MeV. The top panel shows α (filled circles represent the empirical method and open circles represent the Monte Carlo method). The bottom panel shows the ratio of α (Monte Carlo method divided by the empirical method).

isotropic in phase space and then processed through a full GEANT simulation of CLAS. These events were then "smeared" to simulate the drift chamber and time-of-flight resolution. After smearing, the events were processed as normal data.

A comparison between the empirical and Monte Carlo data can be seen for an incident photon energy of 725 MeV in Fig. 5. To perform a statistical comparison for these two data sets, the bottom panel of Fig. 5 (Monte Carlo/empirical) was fit with a polynomial of zero order over the $\cos\theta^\pi_{\rm c.m.}$ range of -0.85 to 0.45. For angles above this range, there were not enough empirical events, after rebinning to the π^0 reaction, to perform a reliable comparison. For $\cos\theta^\pi_{\rm c.m.} < -0.9$, the Monte Carlo did not agree well with the empirical method, and, for this reason, points with $\cos\theta^\pi_{\rm c.m.} < -0.9$ were left out of the subsequent steps of analysis. The zero-order result of the fit is called the "acceptance and efficiency ratio." The ratio of empirical to Monte Carlo for each energy and $\cos\theta^\pi_{\rm c.m.}$ bin (within 0.65 GeV $\leq E_\gamma \leq$ 1.8 GeV and $-0.9 < \cos\theta^\pi_{\rm c.m.} < 0.5$) was placed in a histogram, and then fit with a Gaussian. The center of the Gaussian was found to be 1.0012 ± 0.002, with standard deviation 0.0312 ± 0.016, and reduced $\chi^2 = 0.76$, demonstrating our ability to find and correct for inefficiencies and acceptance.

With this confirmation of the Monte Carlo validity, for $-0.9 < \cos\theta^\pi_{\rm c.m.} < 0.5$ and 0.65 GeV $\leq E_\gamma \leq$ 1.8 GeV (and assuming the validity for all other energies and $-0.9 < \cos\theta^\pi_{\rm c.m.} < 0.9$), the acceptance and efficiency for each kinematic bin for the reaction $\gamma\ p \rightarrow p\ \pi^0$ was obtained by generating 10^7 events (weighted by the cross sections given by the SAID solution [20]). The ratio of processed events, to the number generated, for a given bin, served as a measure of the acceptance and efficiency.

F. Sector-by-sector comparison

The CLAS has six sectors that are nominally identical, but these sectors, in fact, differ relative to each other in acceptance and detection efficiency due to differences that either initially existed in their construction or by various changes and differences that have arisen over time since they were first installed. A sector-by-sector comparison of the differential cross sections was performed to check the consistency of the extracted cross sections. Since the Monte Carlo simulation should reflect sector-by-sector changes in the detector arising from, for example, broken drift chamber wires and time-of-flight paddles, a sector-by-sector comparison of the differential cross section explores the reliability of the Monte Carlo simulation with respect to these detector irregularities. A typical sector comparison plot is shown in Fig. 6. The plot shows the differential cross sections of each sector of CLAS divided by the average over all sectors. An examination of these plots for each energy revealed no

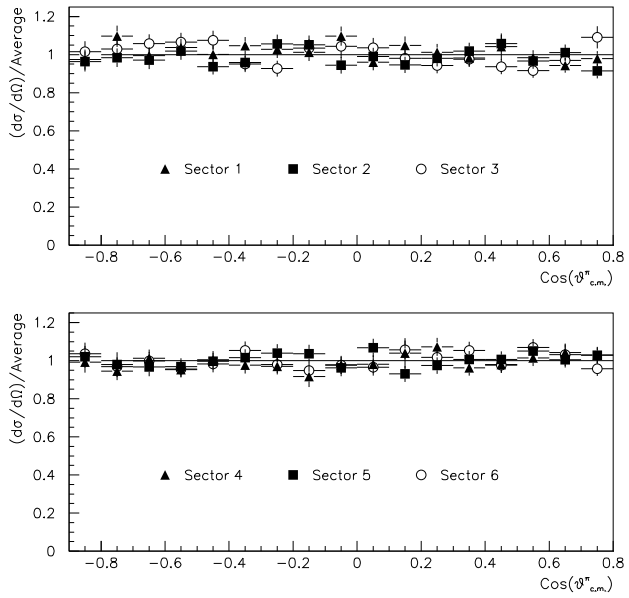

FIG. 6: Differential cross sections for each sector divided by the average over all CLAS sectors ($E_\gamma = 1.025$ GeV) for the reaction $\gamma\ p \to p\ \pi^0$.

systematic shifts visible in the differential cross section for either E_γ or $\cos\theta^\pi_{\rm c.m.}$.

G. Bin migration

To estimate the systematic error associated with bin migration, the acceptance and efficiency results calculated using SAID-weighted events were compared to acceptance and efficiency results using non-weighted events. For each kinematic bin, the systematic error associated with bin migration would be the uncertainty in the corrected value multiplied by the amount of the correction. Since the amount of the correction was found to be typically less than 1.0%, and always less than 2%, the systematic uncertainty associated with bin migration was assumed to be ignorable.

H. Trigger inefficiency

The determination of a charged particle trigger inefficiency for the data was performed by looking at data from a running period that had a CLAS-detected photon event trigger condition in addition to the CLAS-detected charged particle event trigger described above for the g1c running period. An experimental running period that had both charged particle and photon triggers occurred just before the running period used in this analysis. (This dual trigger running period was called g2a; a more detailed discussion of the g2a experiment can be found in Ref. [21].) By observing events in the g2a running period that had a photon trigger and no charged trigger, yet clearly had a proton detected by CLAS in the event, the inefficiency of the charged particle trigger in CLAS for protons could be determined. This correction was applied to each kinematic bin and was always less than 1.0%.

I. Normalization

In contrast to many of the previously published data sets for $\gamma\ p \to p\ \pi^0$, the data in this analysis were not normalized to previous data for the process or to the SAID solution for any reaction channel. The *absolute photon flux* for the entire tagger photon energy range was determined by measuring the rate of scattered electrons detected in each counter of the focal plane of the bremsstrahlung photon tagger by sampling focal plane hits not in coincidence with CLAS. The detection rate for the scattered electrons was integrated over the lifetime of the experiment and converted to the total number of photons on target for each counter of the tagger focal plane. The tagging efficiency was measured in dedicated runs with a total absorption counter (TAC) downstream of the cryogenic target, which directly counted all photons in the beam. The details of the method can be found in Ref. [22].

IV. UNCERTAINTIES

Having investigated various sources of uncertainties in the analysis, we collect and summarize here the various uncertainties determined for the cross sections obtained in this work.

A. Trigger inefficiency

From the *trigger inefficiency* study given in subsection III.H, an overall estimated systematic uncertainty of 1% for the trigger inefficiency correction factors was taken as a very conservative estimate of the systematic uncertainty associated with the trigger inefficiency.

B. Background subtraction

The uncertainty associated with the *background subtraction* is purely statistical, and these were taken into account on a bin-by-bin basis. No systematic uncertainties for the background subtraction are included.

C. Effects of momentum correction

As noted in Section III.B, a pair of momentum corrections for the rescattered proton was made prior to forming the missing mass spectra. These momentum corrections affect extraction of the π^0 from the missing mass distribution, and can alter the the center-of-mass angle for the scattered proton, sometimes transferring events from one kinematic bin to another ("bin migration"). An estimate of the systematic uncertainty introduced by effects of these momentum corrections can be formed by looking at the magnitude of the momentum correction and the magnitude of the resulting deviation from the optimal value determined by a pull distribution.

To determine the uncertainty associated with the momentum correction, the reaction $\gamma\ p \rightarrow p\ \pi^-\ \pi^+$ was studied using methods described in greater detail in Ref. [19]. The variable z is defined as $z = \Delta p_p/\sigma = \left(p_{p(fit)} - p_{p(measured)}\right)/\sigma$, where $p_{p(fit)}$ represents the best value of the momentum as determined by a kinematic fit for data which does not include the CLAS measured value for the proton momentum, and σ is the standard deviation. The distribution of z was examined by histograming and fitting the results to a Gaussian. Histograms were generated for z from events with and without the momentum correction for the proton. The difference between these means is taken as a measure of the average momentum correction.

The initial (final) mean and standard deviation of the pull distribution were 0.208 and 0.963 (-0.022 and 1.011). The magnitude of the change in the mean before and after the momentum correction is 0.23. The amount that the mean of the distribution is still different from the optimal value of zero is 0.022. This suggests that the momentum correction is only good up to $0.022/0.23 = 0.096$. Thus, we estimate conservatively that the systematic uncertainty in the momentum correction is 10%.

The resulting uncertainty in the cross section due to the uncertainty in the *momentum correction* is taken to be 10% of the absolute value of the difference between the momentum corrected and non-momentum corrected differential cross sections. This uncertainty is typically less than a few percent and is added in quadrature on a bin-by-bin basis.

D. Photon flux normalization

Due to the large number of out-of-time photons used to obtain the photon flux normalization [22], the statistical uncertainties associated with the *photon flux normalization* are always far below 1%. For this reason, an overall 1% uncertainty for the statistical error of the normalization is included as a very conservative estimate of this uncertainty.

Since data collection intervals were taken with two different incident electron beam energies, it is reasonable to compare whether any systematic differences arise between the sets of data taken at these two energies. To make this comparison, a histogram was generated for the ratio R, obtained by taking the differential cross sections of the 3.115 GeV data set and dividing those values by the cross sections obtained in the 2.445 GeV data set, for each kinematic bin. A Gaussian was fit to this histogram, with a resulting centroid of 0.996 ± 0.002. From this comparison, we estimate the systematic uncertainty introduced by combining data sets from the two electron energies to be 0.4%. A fluctuation in the photon flux for differing endpoint energies could be due to the energy calibration of the tagger (including effects due to possible, slight differences in the tagger magnet field map). Since an increase of 27% in initial electron energy (2.445 GeV to 3.115 GeV) causes only a 0.4% standard deviation in the photon flux, a conservative estimate of 1% for the systematic uncertainty in photon flux associated with these *"field-to-field"* differences is used.

The largest source of uncertainty in the normalization is caused by the "tagger efficiency" [6]. The tagger efficiency is essentially a measure of the amount of the tagged photon beam that survives collimation, as determined during normalization runs. The value of the tagger efficiency is dependent upon the electron beam supplied by the accelerator, and will vary on a run-by-run basis determined by the condition of the electron beam tune.

To estimate the effects of fluctuations in the electron beam incident on the radiator of the tagger, we calculate the proton yield, normalized to incident photon flux, for each run, and determine the mean and standard deviation of this normalized yield (assuming Gaussian statistics). The *run-by-run uncertainty* was estimated (see Table I) using the standard deviation of this normalized proton yield, dividing by the mean, to get the fractional variation.

E. Absolute normalization

The systematic uncertainty for the *absolute normalization* is comprised of five parts:

1. uncertainty in the cryogenic target density (discussed in detail in Ref. [23]) and length;
2. statistical error of the normalization (described in the preceding subsection);
3. run-to-run variations in the normalized proton yield (described in the preceding subsection);
4. uncertainty associated with the tagger magnetic field calibration ("field-to-field" differences) in combining the results for the two incident electron energies (described in the preceding subsection); and the
5. uncertainty of the trigger inefficiency (described in subsection III.H).

Table I shows the values for these contributions to the systematic uncertainty of the absolute normalization. After adding items (1), (2), and (3) in quadrature and then linearly adding the remaining contributions, the systematic uncertainty for the normalization is 3.7% and 3.9% for the 2.445 GeV and the 3.115 GeV data sets, respectively. Even when all of the systematic uncertainties of the normalization are simply added together, the resulting uncertainty is 4.4% for the 2.445 GeV data set, and 4.8% for the 3.115 GeV data set. Since the estimated error is never over 5%, the overall systematic uncertainty in the absolute normalization is estimated as having a conservative upper bound value of 5%.

TABLE I: Systematic uncertainties in the absolute normalization.

Data Set	Run-to-Run	Target density	Target length
2.445 GeV	0.98%	0.14%	0.28%
3.115 GeV	1.25%	0.28%	0.28%
Data Set	Field-to-field	Trigger	Statistical
2.445 GeV	$< 1\%$	$< 1\%$	$< 1\%$
3.115 GeV		$< 1\%$	$< 1\%$

V. RESULTS

The differential cross sections obtained here are compared with previous data from MAMI-B [24], GRAAL [25], and CB-ELSA [4] in Figs. 7 through 10.

For incident photon energies E up to 1.275 GeV, the data obtained here are generally in very good agreement with previous data. Above that energy discrepancies between this work and the results of the CB-ELSA Collaboration are seen. The disagreement begins at forward meson scattering angles at E_γ=1.325 GeV, and then begins to appear at other angles as the energy increases, though the differences at larger angles are relatively small. The overall systematic uncertainty for the CB-ELSA measurements is stated to be 5% below 1300 MeV and 15% above that energy. This compares with the roughly 5% systematic uncertainty obtained here. With these estimated uncertainties, the data are in statistical agreement for the larger angles, while the discrepancies at the smallest angles are larger than can be accounted for by systematic uncertainties.

Clearly, additional measurements at forward angles are needed to determine whether the rapid increase suggested by the CB-ELSA data is correct, or whether the more gradual behavior predicted by the fits properly describes the trend of the cross section at forward angles.

VI. AMPLITUDE ANALYSIS OF DATA

Multipole amplitude analyses provide a powerful tool for extracting information about the reaction process in as nearly a model-independent manner as possible [20]. This approach, in turn, facilitates the identification of s-channel resonances involved in the reaction process.

Cross sections from this experiment have been included in, and excluded from, a number of multipole fits to the full SAID database [20] in order to gauge their influence and compatibility with previous measurements. In Table II, the values of χ^2 resulting from these fits are compared to predictions from MAID (MAID05 [26] and MAID03 [27]) and an earlier SAID analysis (SM02) [20]. For the purposes of this discussion, several combinations of data sets and fits are presented. A fit called "FDX6" was determined from the world database such that it includes recent GRAAL [25] and CB-ELSA [4] data but does not include the present CLAS dataset, whereas the "FD16" fit includes the CLAS data. To emphasize the effects of the CLAS data reported here and to minimize the influence of CB-ELSA data, the solution "FA06" is a fit that the weight factor for this data was artificially increased by a factor of 3.

The fits FD16 and FA06, despite having different weights for the CLAS data, are in good agreement with each other; this is not surprising, as the older SM02 fit also follows the CLAS data. As seen in Table II, the description of data by MAID is significantly poorer than by any other fit included in this analysis.

TABLE II: χ^2 comparison of fits to 3 GeV, fit SM02 (to 2.0 GeV) [20], and two recent Mainz fits, MAID05 [26] and MAID03 [27] (to 1650 MeV [28]). See text for details.

Solution	Range (MeV)	χ^2/Data
FA06	3000	55640/25524
FD16	3000	52196/24008
FDX6	3000	49010/23250
SM02	2000	35297/17571
MAID05	1650	141270/21942
MAID03	1650	486266/21942

The FA06 and MAID fits are compared to data over the range of the MAID analysis in Fig. 7. Above this energy limit (1650 MeV), we compare FA06 and the older SM02 solution in Fig. 7. The deviation of MAID03 from data and the SAID fits, above approximately 1 GeV, is known to the Mainz group. The (preliminary) MAID05 fit is much improved. A version to be made publicly available through the MAID website will contain further modifications [29]. The MAID05 and SAID fits are significantly different in the most forward bump/dip structure and at backward angles.

The forward region continues to differ most in Fig. 8, where the fits SM02 and FA06 are compared. At intermediate angles, agreement between the CLAS and

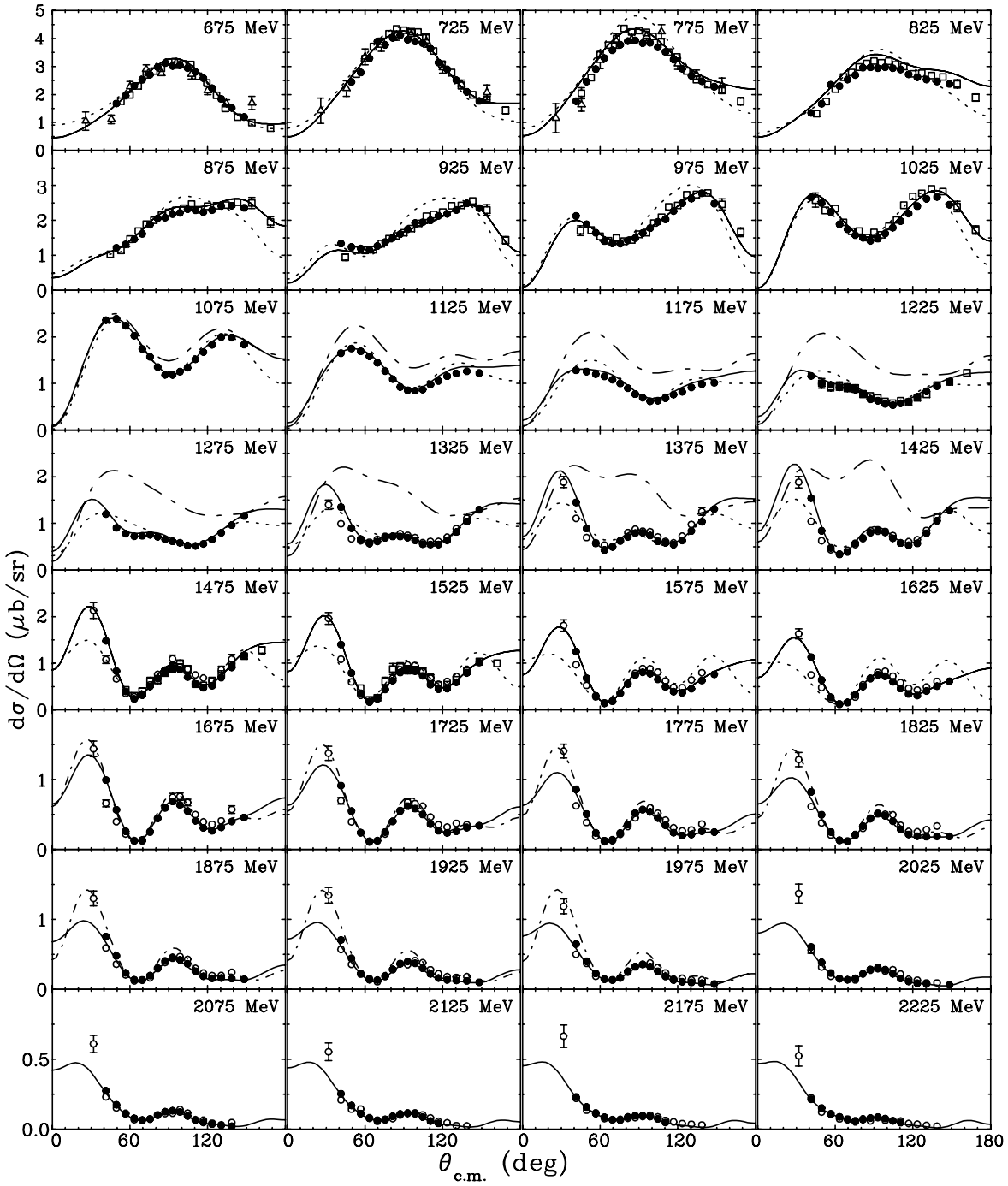

FIG. 7: The differential cross section for $\gamma p \to \pi^0 p$ below $E_\gamma = 2250$ MeV. The angle shown is the pion center-of-mass scattering angle. Solid (short dash-dotted) lines correspond to the SAID FA06 (SM02 [20]) solution. SM02 curves are shown only for E_γ between 1650 and 2000 MeV. Dotted (long dash-dotted) lines give the MAID05 [26] (MAID03 [27]) predictions. MAID03 curves are shown only for E_γ between 1050 to 1450 MeV. Experimental data are from the current measurement (filled circles), MAMI-B [24] (open triangles), GRAAL [25] (open squares), and CB-ELSA [4] (open circles). The plotted experimental data have been selected from energy bins spanning at most 5 MeV.

CB-ELSA datasets is quite good. Note that the older SM02 fit is in perfect agreement with the most forward CB-ELSA measurements, though these data were not included in the fit. The model dependence of this forward region is further explored in Fig. 8. Note that the FDX6 result, including CB-ELSA but *not* CLAS data, is actually in worse agreement with the most forward CB-ELSA measurements. The FA06 fit (which includes the CB-

ELSA points and the data obtained here) yields results that also fall far below the most forward point measured by the CB-ELSA collaboration. While only suggestive, this observation adds some support to the less rapid increase in the differential cross sections implied by the data obtained here.

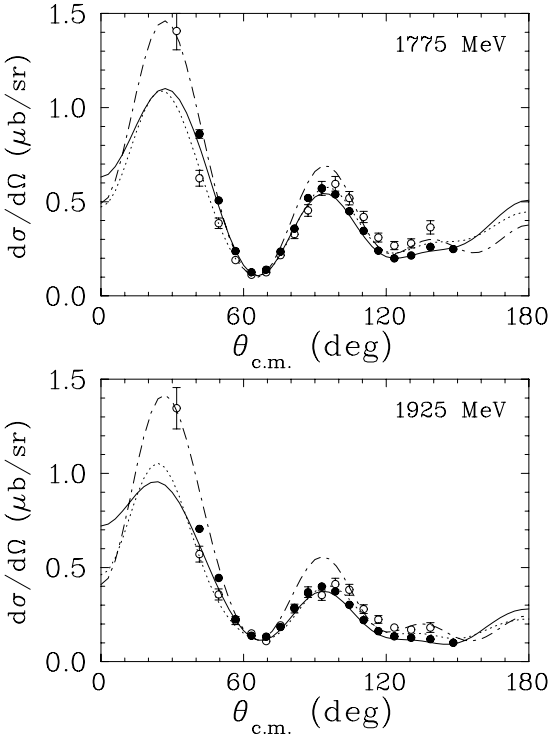

FIG. 8: The differential cross section for $\gamma p \to \pi^0 p$ at E_γ = 1775 and 1925 MeV. The angle shown is the pion center-of-mass scattering angle. Solid (long dash-dotted) lines corresponding to the GW SAID FA06 (SM02 [20]) solution. Dotted lines represent FDX6 results. Experimental data are from the current measurement (filled circles) and CB-ELSA [4] (open circles).

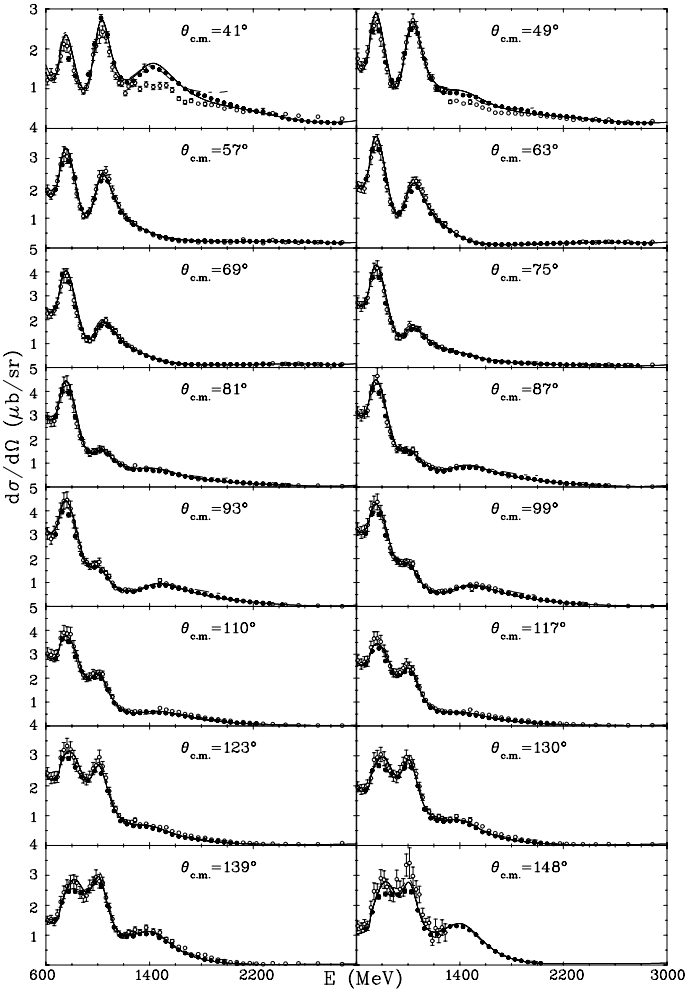

FIG. 9: Fixed angle excitation functions for $\gamma p \to \pi^0 p$. The angle shown is the pion center-of-mass scattering angle. Solid (long dash-dotted) lines corresponding to the GW SAID FA06 (SM02 [20]) solution. Experimental data are from the current measurement (filled circles) and CB-ELSA [4] (open circles).

The present fits have been generated using the most recent GW analysis of pion-nucleon scattering data, which was extended to cover the full resonance region [30]. The upper limit on the photon energy is 3 GeV (as compared to 2 GeV for SM02 [20]), incorporating the full CLAS dataset determined here. In Figs. 9 and 10, we display the energy dependence of cross sections at fixed angle. This view most clearly shows the kinematic region and scale of disagreement between the CLAS and CB-ELSA datasets. Also apparent is the transition, between 2 and 3 GeV, to a region where the cross sections have a nearly energy-independent structure.

VII. RESONANCE COUPLINGS

Multipoles from the FA06 fit are compared to the earlier SAID (SM02) determinations in Figs. 11 and 12. As suggested by the falling cross sections, the multipoles are either flat or rapidly decreasing in magnitude at the upper energy limit (e.g., the $E_{2-}^{1/2}$ and $E_{1+}^{3/2}$ multipoles). The extension to higher energies provided by this data set has resulting in a smoothing of some structures found in the 2 GeV limit of the SM02 solution (see, in particular, the $E_{2-}^{3/2}$ and $E_{2+}^{3/2}$ multipoles). Comparisons with the MAID05 solution are given in Figs. 13 and 14.

Resonance contributions have been fit and the resulting helicity amplitudes are presented in Table III. Values for the resonance mass W_R, width Γ, and branching fraction ($\Gamma_{\pi N}/\Gamma$) for the various resonances were taken from the recent SAID analysis of pion-nucleon elastic scattering [30]. The electromagnetic resonance couplings were extracted using a form

$$B(W)(1 + iT_{\pi N}) + T_{BW}e^{i\phi}, \qquad (1)$$

wherein $T_{\pi N}$ was the associated full pion-nucleon T-

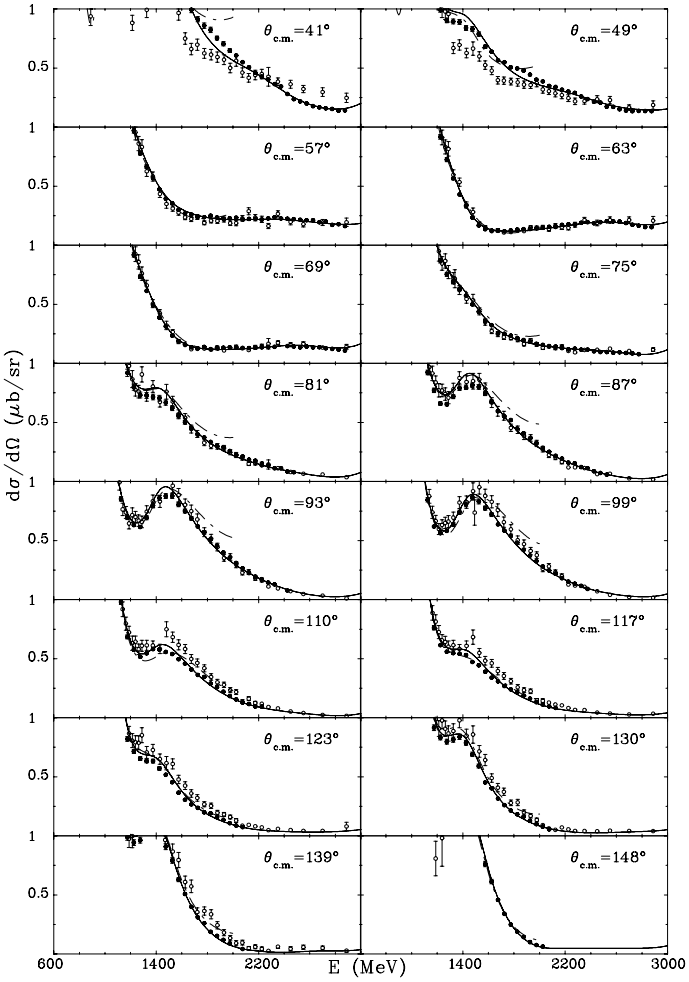

FIG. 10: Fixed angle excitation functions for $\gamma p \to \pi^0 p$ below 1μb/sr. Notation as in Fig. 9.

matrix and T_{BW} was a Breit-Wigner parametrization of the resonance contribution. This is similar to the MAID form, but allows for a more flexible polynomial function to account for the non-resonant contributions from channels such as $\pi\Delta$, as described in Ref. [31].

The uncertainties for the helicity amplitudes given in Table III extracted in the FA06 analysis correspond to a χ^2 increase of 9 in the fit. This uncertainty is thus purely statistical and does not account for subjectivity in the resonance extraction and selection of the energy range used in the resonance fit. Table IV compares χ^2 values from FA06 and the resonance fits over corresponding energy ranges.

Most of the resonance couplings determined in this analysis generally are in fair agreement with the PDG averages, but there are significant disagreements for the $N(1650)$ and $N(1720)$. The $N(1650)$ couplings are particularly difficult to extract as there is an overlapping resonance (the $N(1535)$ resonance) below this state and possibly a third resonance slightly higher in energy. The $N(1720)$ coupling, quoted by the PDG, is not clearly determined even in sign. Furthermore, the multipoles associated with this state have also changed dramatically in the extension to 3 GeV, as can be seen in Fig. 11.

TABLE III: Resonance parameters for N* and Δ^* from the SAID fit to the πN data [30] (second column) and helicity amplitudes $A_{1/2}$ and $A_{3/2}$ (in $[(\mathrm{GeV})^{-1/2} * 10^{-3}]$ units) from the FA06 solution (first row) and average values from the PDG06 [1] (second row).

Resonance	πN SAID	$A_{1/2}$	$A_{3/2}$
$N(1535)S_{11}$	W_R=1547 MeV	91.0±2.2	
	Γ=188 MeV	90±30	
	Γ_π/Γ=0.36		
$N(1650)S_{11}$	W_R=1635 MeV	22.2±7.2	
	Γ=115 MeV	53±16	
	Γ_π/Γ=1.00		
$N(1440)P_{11}$	W_R=1485 MeV	−50.6±1.9	
	Γ=284 MeV	−65±4	
	Γ_π/Γ=0.79		
$N(1720)P_{13}$	W_R=1764 MeV	96.6±3.4	−39.0±3.2
	Γ=210 MeV	18±30	−19±20
	Γ_π/Γ=0.09		
$N(1520)D_{13}$	W_R=1515 MeV	−28.0±1.9	143.1±2.0
	Γ=104 MeV	−24±9	166±5
	Γ_π/Γ=0.63		
$N(1675)D_{15}$	W_R=1674 MeV	18.0±2.3	21.2±1.4
	Γ=147 MeV	19±8	15±9
	Γ_π/Γ=0.39		
$N(1680)F_{15}$	W_R=1680 MeV	−17.3±1.4	133.6±1.6
	Γ=128 MeV	−15±6	133±12
	Γ_π/Γ=0.70		
$\Delta(1620)S_{31}$	W_R=1615 MeV	49.6±2.2	
	Γ=147 MeV	27±11	
	Γ_π/Γ=0.32		
$\Delta(1232)P_{33}$	W_R=1233 MeV	−139.1±3.6	−257.6±4.6
	Γ=119 MeV	−135±6	−250±8
	Γ_π/Γ=1.00		
$\Delta(1700)D_{33}$	W_R=1695 MeV	125.4±3.0	105.0±3.2
	Γ=376 MeV	104±15	85±22
	Γ_π/Γ=0.16		
$\Delta(1905)F_{35}$	W_R=1858 MeV	21.3±3.6	−45.6±4.7
	Γ=321 MeV	26±11	−45±20
	Γ_π/Γ=0.12		

The good agreement between the fit and PDG parameters seen for the $N(1535)$ resonance also deserves some comment. The large PDG error band was given mainly to account for the spread in determinations from pion and eta photoproduction analyses. This discrepancy has largely disappeared [32]. However, the same qualifications addressed to the $N(1650)$ resonance apply here as well. Model dependence in this extraction is certainly larger than the statistical error quoted in Table III.

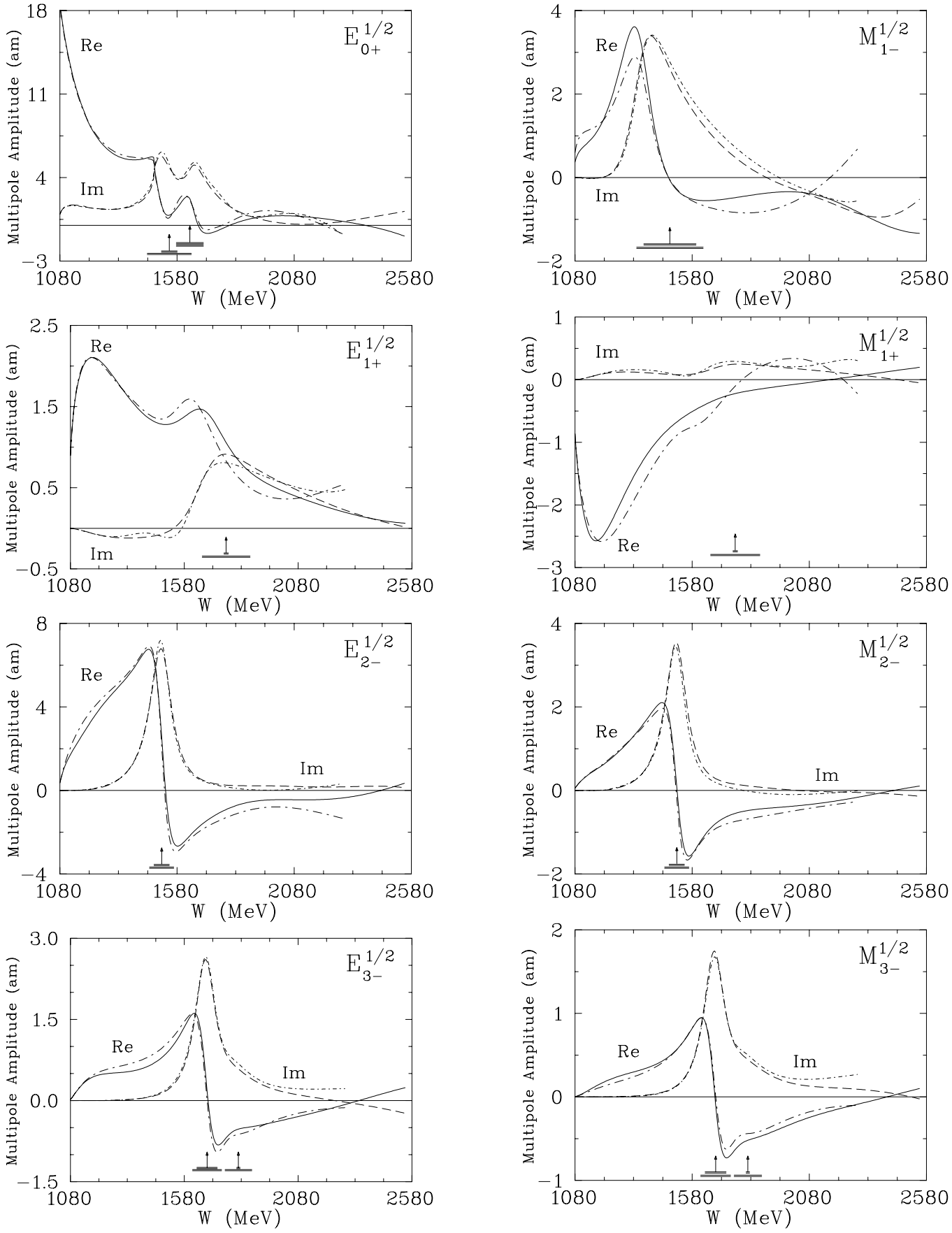

FIG. 11: Multipole amplitudes from threshold to $E_\gamma = 3$ GeV for isospin 1/2. Solid (dashed) curves give the real (imaginary) parts of amplitudes corresponding to the SAID FA06 solution. The previous SAID SM02 solution [20] is given by long dash-dotted (real part) and short dash-dotted (imaginary part) lines. Vertical arrows indicate W_R and horizontal bars show full Γ and partial widths for $\Gamma_{\pi N}$ associated with the SAID πN solution SP06 [30].

TABLE IV: Comparison of the resonance fit and FA06 against data for the isospin 1/2 and 3/2 baryon resonances (see text and associated Table III). The "Data" corresponds to the number of experimental data points in the given range of the W_{min} and W_{max} limits. Energy limits are those used in the most recent πN resonance extractions [30].

Resonance	W_{min} (MeV)	W_{max} (MeV)	Fit χ^2	FA06 χ^2	Data
$N(1535)S_{11}$	1490	1590	7129	7546	3552
$N(1650)S_{11}$	1620	1770	6013	6520	2588
$N(1440)P_{11}$	1350	1550	13434	13752	6897
$N(1720)P_{13}$	1650	1790	5520	5717	2514
$N(1520)D_{13}$	1480	1560	7252	7554	3481
$N(1675)D_{15}$	1610	1730	5900	6139	2406
$N(1680)F_{15}$	1620	1730	5359	5625	2187
$\Delta(1620)S_{31}$	1570	1680	5764	6018	2475
$\Delta(1232)P_{33}$	1180	1270	6303	6630	3351
$\Delta(1700)D_{33}$	1550	1750	7285	7577	3064
$\Delta(1905)F_{35}$	1770	1920	3930	4089	1787

Given the smooth behavior exhibited by the excitation functions in Figs. 9 and 10, the CLAS cross sections provide no hint of "missing" resonance structure between 2 and 3 GeV. The SAID fits implicitly contain only those resonances found in the corresponding SAID analysis of elastic pion-nucleon scattering data. No change in the form of the SAID photoproduction fit was found to be necessary. In contrast, the CB-ELSA fit required many additional resonance contributions, some of which are 1- and 2-star rated PDG states, as well as a new N(2070) resonance. One possible explanation is apparent in Fig. 10, which shows the CLAS data to be somewhat smoother than the CB–ELSA excitation functions. Model-dependence in the separation of resonance and background contributions is also a critical factor. This uncertainty can be reduced through measurements of further (polarized) data.

VIII. CONCLUSION

The differential cross sections for the reaction $\gamma\ p \rightarrow p\ \pi^0$ for incident photon energies between 0.675 and 2.875 GeV have been measured. These measurements have been compared to existing data, mainly from the CB-ELSA Collaboration. The overall agreement is excellent, though statistically significant disagreement is evident in some cases between that data and a few values obtained here in the forward direction. The variation of fits in the forward region suggest further measurements at those angles would be very useful. As shown in Figs. 9 and 10, both the SAID fit SM02, developed prior to the publication of both the CB-ELSA and CLAS data, and FA06 (including both sets) appear to favor the most forward CLAS measurements over the CB-ELSA measurements.

Multipole analyses incorporating the CLAS data and extending to 3 GeV now appear more smooth near the 2 GeV limit of previous fits, tending to be relatively featureless and rapidly decreasing above this energy. At energies above 2 GeV and outside of the angular range constrained by CLAS data, the fits were found to be unstable. More progress will require precise measurements in that angular region, and also the availability of polarization observables of a similar quality and coverage. Corresponding data from $n\pi^+$ photoproduction are also clearly required to make an isospin decomposition. A partial wave analysis performed in this work using only "4-star" resonances at or below W=1910 MeV satisfactorily described the data.

Acknowledgments

The authors gratefully acknowledge the Jefferson Lab Accelerator Division staff. This work was supported by the National Science Foundation, the Department of Energy (DOE), the Deutsche Forschungsgemeinschaft (through an Emmy Noether grant to U.T.), the French Centre National de la Recherche Scientifique and Commissariat à l'Energie Atomique, the Italian Istituto Nazionale di Fisica Nucleare, and the Korean Science and Engineering Foundation. The Southeastern Universities Research Association (SURA) operated Jefferson Lab for DOE under contract DE-AC05-84ER40150 during this work.

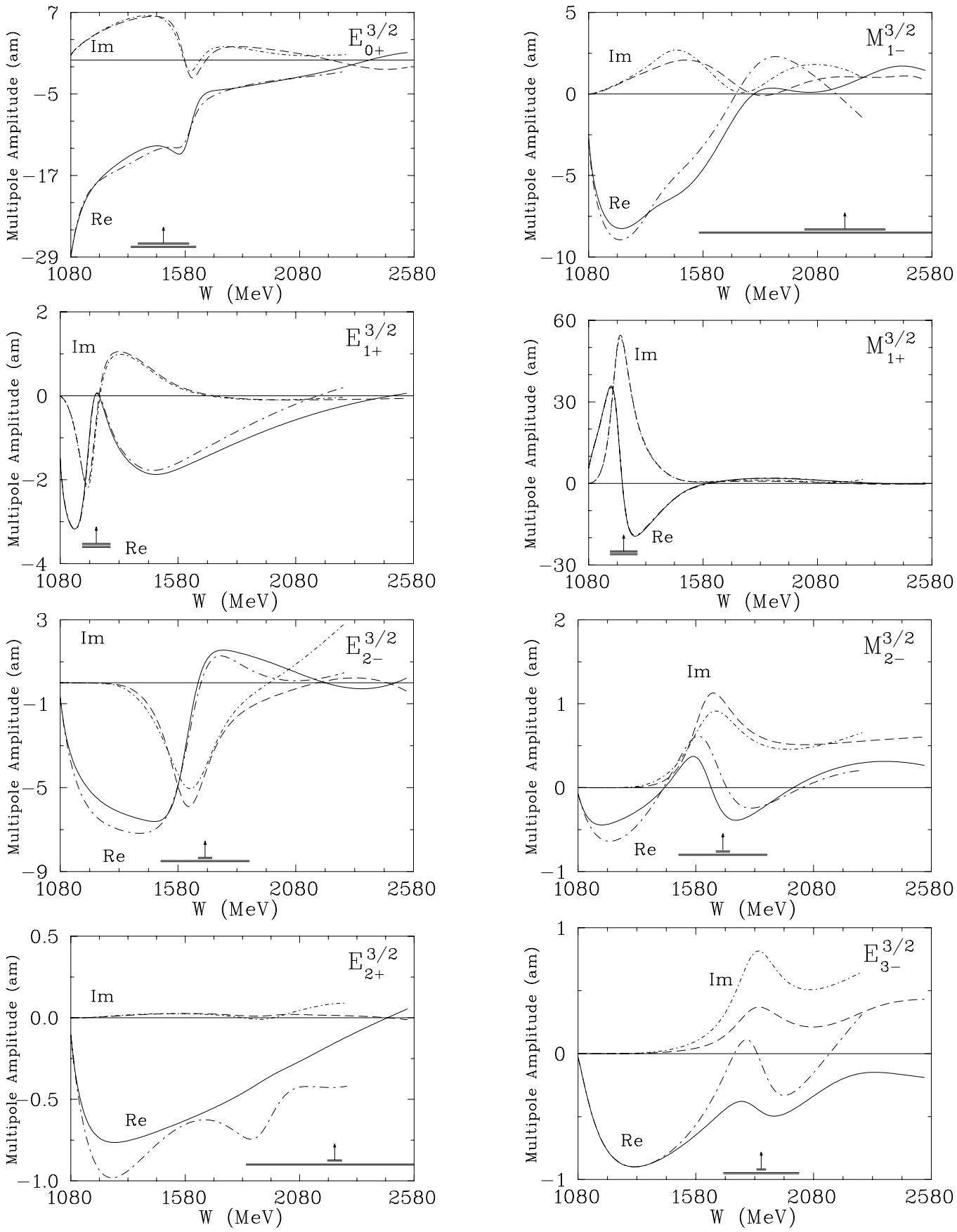

FIG. 12: Multipole amplitudes from threshold to $E_\gamma = 3$ GeV for isospin 3/2. Notation as in Fig. 11.

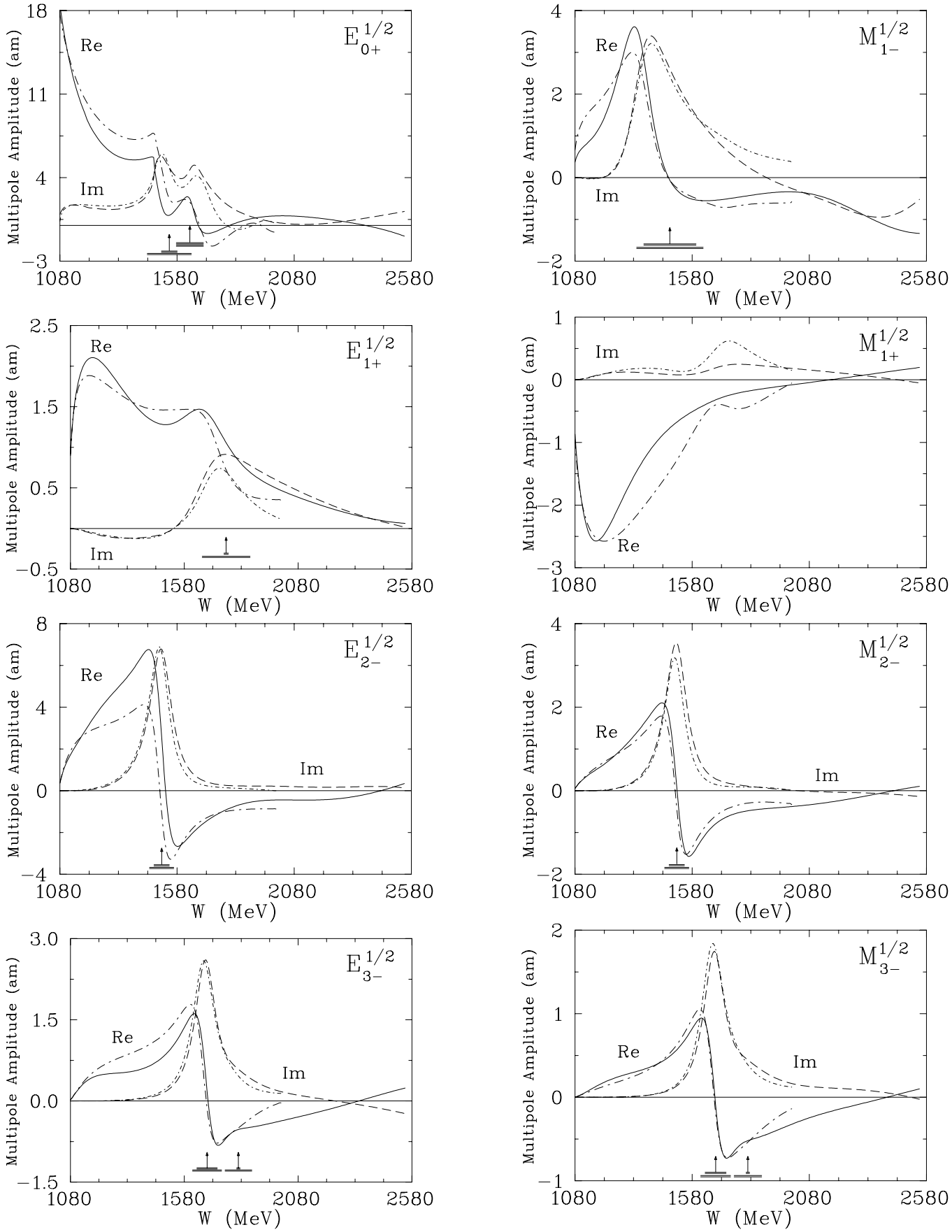

FIG. 13: Multipole amplitudes from threshold to $E_\gamma = 3$ GeV for isospin 1/2. Solid (dashed) curves give the real (imaginary) parts of amplitudes corresponding to the SAID FA06 solution. The MAID05 solution [26] is given by long dash-dotted (real part) and short dash-dotted (imaginary part) lines.

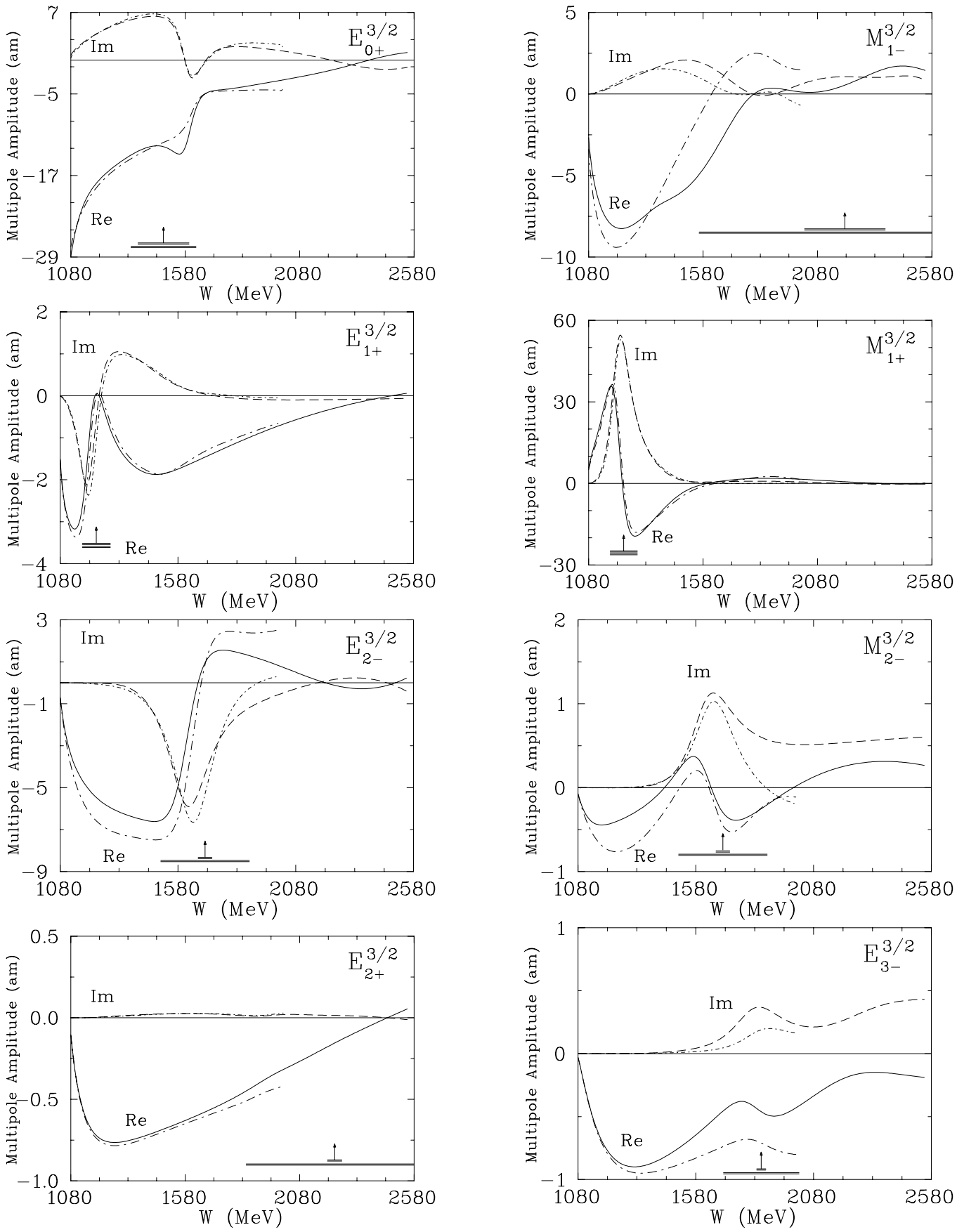

FIG. 14: Multipole amplitudes from threshold to $E_\gamma = 3$ GeV for isospin 3/2. Notation as in Fig. 13.

[1] W.-M. Yao *et al.* (*Review of Particle Physics*), J. Phys. G **33**, 1 (2006).

[2] K. Wijesooriya *et al.* (JLab Hall A Collaboration), Phys. Rev. C **66**, 034614 (2004);
R. A. Arndt, I. I. Strakovsky, and R. L. Workman, Phys. Rev. C **67**, 048201 (2003) [nucl-th/0212055].

[3] L. Y. Zhu *et al.* (JLab Hall A Collaboration), Phys. Rev. C **71**, 044603 (2005) [nucl-ex/0409018].

[4] O. Bartholomy *et al.* (CB–ELSA Collaboration), Phys. Rev. Lett. **94**, 012003 (2005) [hep–ex/0407022]; H. van Pee *et al.* (CB–ELSA Collaboration), Eur. Phys. J A **31**, 61 (2007).

[5] B. Mecking *et al.* (CLAS Collaboration), Nucl. Instr. Meth. A **503**, 513 (2003).

[6] D. I. Sober *et al.*, Nucl. Inst. and Meth. in Phys. Res. A **440**, 263 (2000).

[7] The CLAS Database archives all data from CLAS. It is reachable via http://clasweb.jlab.org/physicsdb.

[8] R. Bradford *et al.* (CLAS Collaboration), Phys. Rev. C **73**, 035202 (2006) [nucl-ex/0509033].

[9] M. Dugger *et al.* (CLAS Collaboration), Phys. Rev. Lett. **96**, 062001 (2006) [nucl-ex/0512019].

[10] S. Strauch *et al.* (CLAS Collaboration), Phys. Rev. Lett. **95**, 162003 (2005) [hep-ex/0508002].

[11] J. W. C. McNabb *et al.* (CLAS Collaboration), Phys. Rev. C **69**, 042201 (2004) [nucl-ex/0305028].

[12] M. Battaglieri *et al.* (CLAS Collaboration), Phys. Rev. Lett. **90**, 022002 (2002) [hep-ex/0210023].

[13] M. Dugger *et al.* (CLAS Collaboration), Phys. Rev. Lett. **89**, 222002 (2002).

[14] M. Battaglieri *et al.* (CLAS Collaboration), Phys. Rev. Lett. **87**, 172002 (2001) [hep-ex/0107028].

[15] E. Anciant *et al.* (CLAS Collaboration), Phys. Rev. Lett. **85**, 4682 (2000) [hep-ex/0006022].

[16] S. Taylor *et al.* (CLAS Collaboration), Nucl. Instr. Meth. A **462**, 484 (2001).

[17] E. S. Smith *et al.* (CLAS Collaboration), Nucl. Instr. Meth. A **432**, 265 (1999).

[18] E. Pasyuk, CLAS Note 2007-008, www1.jlab.org/ul/Physics/Hall-B/clas/public/2007-008.pdf.

[19] M. Williams, D. Applegate, and C. A. Meyer, CLAS Note 2004-017, www1.jlab.org/ul/Physics/Hall-B/clas/public/2004-017.pdf.

[20] R. A. Arndt, W. J. Briscoe, I. I. Strakovsky, and R. L. Workman, Phys. Rev. C **66**, 055213 (2002) [nucl–th/0205067]; gwdac.phys.gwu.edu.

[21] M. Mirazita *et al.* (CLAS Collaboration), Phys. Rev. C **70**, 014005 (2004) [nucl-ex/0405019].

[22] J. Ball and E. Pasyuk, CLAS Note 2005-002, www1.jlab.org/ul/Physics/Hall-B/clas/public/2005-002.pdf.

[23] R. Bradford and R. A. Schumacher, CLAS Note 02-003, www.jlab.org/Hall-B/notes/clas_notes02/02-003.pdf.

[24] B. Krusche *et al.*, Eur. Phys. J. A **6**, 309 (1999).

[25] O. Bartalini *et al.* (GRAAL Collaboration), Eur. Phys. J. A **26**, 399 (2005).

[26] MAID05 version; D. Drechsel, O. Hanstein, S. S. Kamalov, and L. Tiator, Nucl. Phys. **A645**, 145 (1999) [nucl-th/9807001]; S. S. Kamalov and L. Tiator, private communication.

[27] MAID03 version; D. Drechsel O. Hanstein, S. S. Kamalov, and L. Tiator, Nucl. Phys. **A645**, 145 (1999) [nucl-th/9807001]; see MAID03 at www.kph.uni-mainz.de/MAID/.

[28] L. Tiator, talk given at: *9th International Symposium on Meson-Nucleon Physics and the Structure of the Nucleon (MENU2001), Washington, DC, USA, July, 2001*, private communication, 2001.

[29] S. S. Kamalov, private communication, 2006.

[30] R. A. Arndt, W. J. Briscoe, I. I. Strakovsky, and R. L. Workman, Phys. Rev. C **74**, 045205 (2006) [nucl–th/0605082].

[31] R. L. Workman, Phys. Rev. C **74**, 055207 (2006) [nucl-th/0510025].

[32] This discrepancy was already absent in our previous analysis [20] but the published value was incorrect due to an error in the SAID code.